ACS Chemical Neuroscience

pubs.acs.org/chemneuro

Research Article

Development of a Dual Fluorescent and Magnetic Resonance False Neurotransmitter That Reports Accumulation and Release from Dopaminergic Synaptic Vesicles

Michael R. Post, Wei-Li Lee, Jia Guo, Dalibor Sames,* and David Sulzer*

Cite This: *ACS Chem. Neurosci.* 2021, 12, 4546−4553

Read Online

ACCESS | Metrics & More | Article Recommendations

ABSTRACT: Myriad neuropsychiatric disorders are due to dopamine dysfunction. However, understanding these disorders is limited by our ability to measure dopamine storage and release. Fluorescent false neurotransmitters (FFNs), small-molecule dyes that co-transit through the synaptic vesicle cycle, have allowed us to image dopamine in cell culture and acute brain slice, but *in vivo* microscopy is constrained by the biopenetrance of light. Here, we adapt FFNs into magnetic resonance false neurotransmitters (MFNs). The design principles guiding MFNs are (1) the molecule is a valid false neurotransmitter and (2) it has a ^{19}F-substituent near a pH-sensing functional group, which (3) has pK_a close to 6 so that the probe within vesicles is protonated. We demonstrate that MFN103 meets these criteria. While a magnetic resonance spectroscopy (MRS) signal was too low for measurement *in vivo* with the current technology, in principle, MFNs can quantify neurotransmitters within and without synaptic vesicles, which may underlie noninvasive *in vivo* analysis of dopamine neurotransmission.

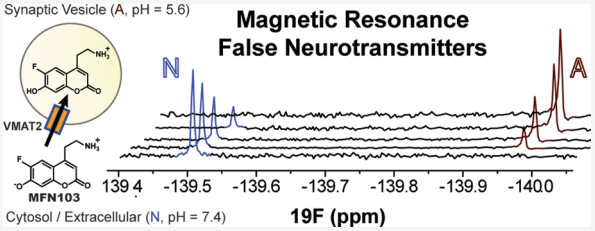

KEYWORDS: *dopamine, neurotransmitter sensor, MRS, synaptic vesicles, Parkinson's disease, striatum*

INTRODUCTION

Dopamine, a small-molecule neurotransmitter, is involved in motor- and reward-directed behaviors and is implicated in many neuropsychiatric disorders.[1,2] For example, a body of evidence indicates that schizophrenia is characterized by increased dopamine storage and release in the striatum, whereas Parkinson's disease is typically diagnosed by motor symptoms that appear when ∼80% percent of striatal dopaminergic axons have degenerated.[3,4] Our understanding of the progression and mechanisms underlying these diseases is limited, however, by our ability to image dopamine.[5] For example, detecting dopamine neuron loss *via* measurement of dopamine storage and release prior to the emergence of symptoms would allow for earlier diagnosis and therefore intervention, as well as a quantitative approach to monitor disease progress following any intervention.

Dopamine is accumulated and released from synapses *via* synaptic vesicles.[6] After synthesis from tyrosine by the enzymes tyrosine hydroxylase (TH) and aromatic L-amino acid decarboxylase, it is sequestered into synaptic vesicles by the vesicular monoamine transporter (VMAT2).[7] This transporter operates on a pH gradient—exchanging two protons for one dopamine molecule—which is established by a vesicular ATPase (Figure 1B).[8,9] The synaptic vesicles fuse with the plasma membrane to release their content, bathing the extracellular space in dopamine. From there, dopamine is transported back into the axon by the dopamine active transporter (DAT), where it reaccumulates in vesicles.[10,11] Dopamine, like other monoamine neurotransmitters including norepinephrine, activates G protein-coupled receptors rather than ligand-gated ion channels, a characteristic that has complicated our understanding and study of dopaminergic synapses.[12] Many tools have been developed recently, including those based on fluorescence, PET/SPECT (such as recently approved-for-the-clinic DATSCAN), and MRI modalities, to either directly measure release or indirectly measure storage, but none achieve quantitative measurement of both storage and release.[13−16] Fluorescent probes such as dLight and GRAB$_{DA}$ protein sensors or the nIRCat nanoparticle sensor experience a gain in fluorescence intensity in the presence of dopamine, but these require optical fiber implants in mice or are limited to cell culture.[17−19] An MRI dopamine sensor based on cytochrome P450—BM3h—is able to sense dopamine release but, like dLight and GRAB$_{DA}$, requires the introduction of a protein sensor and only measures dopamine release.[20,21] A small-molecule approach would avoid this

Received: August 30, 2021
Accepted: November 11, 2021
Published: November 24, 2021

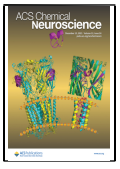

https://doi.org/10.1021/acschemneuro.1c00580
ACS Chem. Neurosci. 2021, 12, 4546−4553

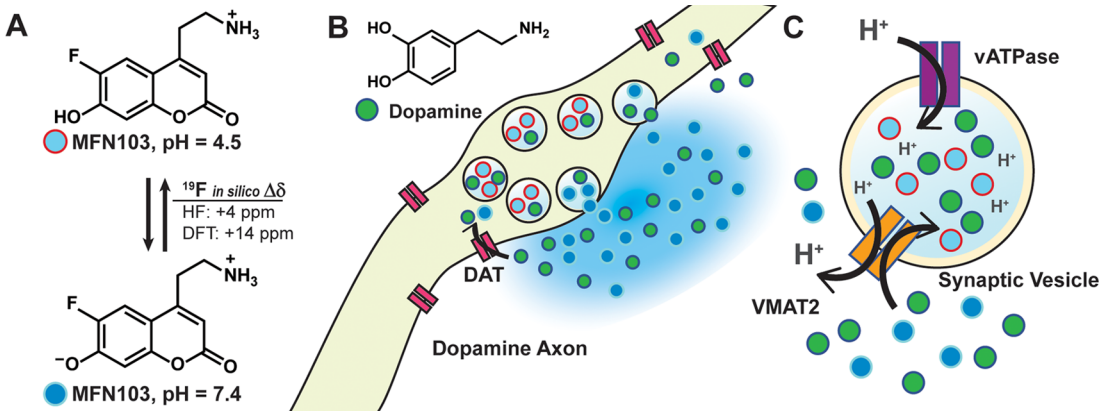

Figure 1. MFN103 schematic. (A) Structures and acid−base equilibrium of MFN103 and the corresponding Hartree−Fock- and DFT-calculated changes in chemical shift; (B) dopamine's chemical structure and an illustration of its synaptic vesicle cycle, as well as how false neurotransmitters hijack this cycle to image dopamine storage and release; and (C) schematic of a dopaminergic synaptic vesicle, demonstrating how vATPase acidifies the vesicles and VMAT2 uses this proton gradient to accumulate dopamine and FNs.

requirement and has the capacity to measure both storage and release, and one without requiring ionizing radiation (such as PET/SPECT tools) would be an invaluable addition tool for diagnosing and monitoring dopaminergic disease progress and interventions.

The fluorescent false neurotransmitters (FFNs), developed by our laboratories, have been useful for imaging both storage and release in cultured primary neurons, in *ex vivo* brain slice, and *in vivo*. These small-molecule probes operate by hijacking the synaptic vesicle cycle, serving as DAT and/or VMAT2 substrates (Figure 1); importantly, they do not activate post-synaptic dopamine receptors, as doing so would make the potentially high concentrations necessary for imaging intolerable in eventual patients.[22] An added layer of functionality was achieved by introducing a pH-sensitive handle to the FFNs, allowing us to distinguish the probe sequestered in synaptic vesicles—which have a low pH established by vATPase—from that which is released.[23,24] These compounds become brighter at higher pH, and so, when released from the acidic interior of the synaptic vesicle (often estimated as ∼ pH 5.6, although the small volume of a synaptic vesicle would reach this value with only a single free proton)[11] to the relatively neutral pH of extracellular milieu, there is a rapid fluorescent flash that indicates exocytosis: we call these compounds *flashing FFNs*.[23]

Recently, we reported the first *in vivo* use of a flashing FFN using the pH-sensitive FFN270 in the cortex.[24] This was enabled by FFN270's preference for uptake by the norepinephrine transporter over DAT, allowing it to be imaged in the cortex *via* a cranial window and an *in vivo* two-photon microscopy setup. Due to FFN270's pH sensitivity, its release was observed following depolarization *via* KCl as well as amphetamine, which has multiple effects on monoamine neurotransmitters including neutralization of synaptic vesicle pH.[25] Translating *in vivo* imaging to dopamine neurons using, for example, the pH-sensitive FFN102 is complicated because the axons are mostly in deeper brain structures, and it is presently technically challenging to deliver fluorescent excitation and small-molecule probes to the same location.

Therefore, we sought to extend the FFN concept into a more biopenetrant modality, namely, magnetic resonance spectroscopy (MRS). MRS is similar to magnetic resonance imaging (MRI) except that rather than shading each voxel based on relaxation times, the free induction decay is Fourier-transformed to produce a spectrum where each peak location, or chemical shift, is related to that corresponding nucleus' chemical environment.[26,27] MRS is completely analogous to an organic chemist's use of NMR and has been used to identify brain concentrations of common neurotransmitters and analytes such as glutamate, GABA, and *N*-acetylaspartate.[28,29] Dopamine itself cannot be imaged by MRS due to a low relative concentration in the brain and a lack of CH_3− groups. Moreover, the proton space is quite crowded in brain MRS, and detection of exogenous probes can be difficult.

With this in mind, we chose to develop a probe that can be measured by 19F-MRS. This has several advantages: 19F is 100% abundant in nature but completely absent in the brain; 19F has a gyroscopic ratio of 0.95 relative to protons, making its signal strength and collection times comparable to protons; and 19F experiences a wide range of chemical shifts, spanning over 100 ppm. Although not commonly used, there is a precedent for 19F-MRS/I, including measuring fluorinated dopamine in guinea pig neural sacks, a report that followed the metabolism of 5-fluorouracil into fluoro-β-alanine in a patient with a liver tumor, and recently, development of a fluorinated congo red derivative that can detect amyloid beta plaques.[30−32]

Based on these foundational studies, as well as previous work with FFNs, we established three criteria to develop magnetic-resonant false neurotransmitters (MFNs):

1. A small molecule that is a DAT and/or VMAT2 substrate
2. pH-sensitive so that it is protonated in synaptic vesicles and deprotonated outside so that
3. a nearby fluorine handle experiences a resolvable change in chemical shift with the corresponding change in pH.

If all three criteria are satisfied, we would expect to observe a neutral peak when MFN is delivered to the dopamine neurons that, as it is sequestered into synaptic vesicles, diminishes as an acidic peak appears. Following stimuli that release dopamine, we would then expect this to reverse, with the acidic peak decreasing and the neutral peak increasing.

Here, we report a first example of an MFN, MFN103, which satisfies these criteria *in silico*, *in vitro*, and *ex vivo* and demonstrates the general concept of MFNs. We also discuss obstacles to be overcome for successful application of MFNs *in vivo*.

https://doi.org/10.1021/acschemneuro.1c00580
ACS Chem. Neurosci. 2021, 12, 4546−4553

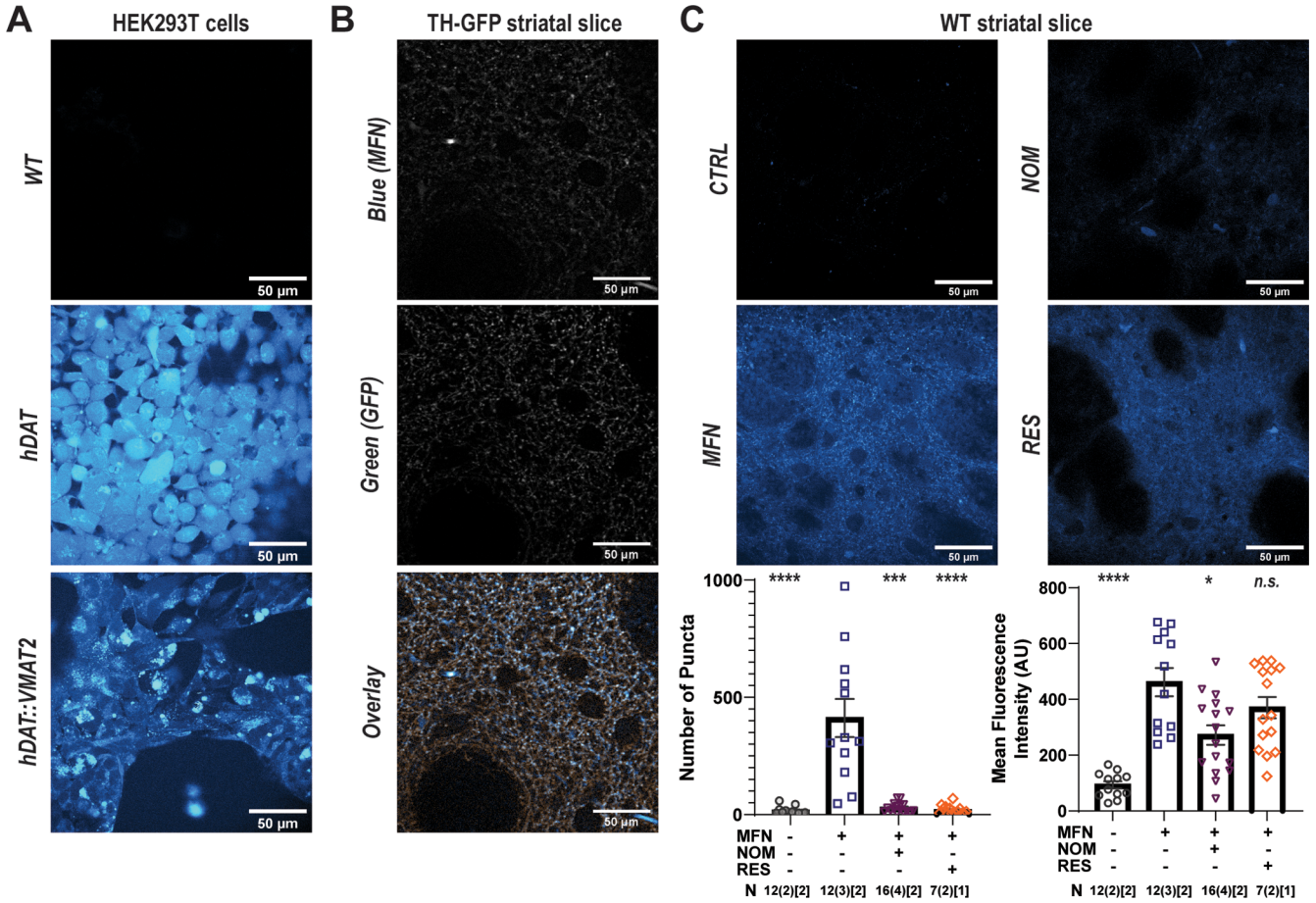

Figure 2. MFN103 is a false neurotransmitter. Two-photon micrographs of (A) HEK293T cells that are WT or expressing DAT and/or VMAT2 incubated with MFN103; (B) acute striatal slices from TH-driven GFP mice incubated in MFN with blue and green channels shown in the gray scale and a composite to demonstrate colocalization; (C) acute WT mouse striatal slices that were incubated in vehicle alone (CTRL), MFN, or MFN with nomifensine (NOM) or reserpine (RES), quantified in the bar graphs below for the number of puncta in the field of view and the mean fluorescence intensity of the tissue. Statistics: error bars represent the standard error of the mean; a Kruskal–Wallis test (non-parametric one-way ANOVA) was used to test significance, with all means compared to the MFN-only condition; *: $p < 0.05$, ***: $p < 0.001$, ****: $p < 0.0001$, and n.s.: not significant; and the N for each condition is notated as images (slices)[animals] and each symbol represents an individual image.

RESULTS AND DISCUSSION

We recently developed a compound related to FFN102 (see the Supporting Information section of Lee *et al.*—referred to as mini103 in that study) that consists of a fluorescent coumarin scaffold with a 4-ethylamino group (thought to confer VMAT2 specificity), along with 6-hydroxy (imbuing pH sensitivity) and 5-fluoro (to attenuate the pK_a) substituents (Figure 1A).[23] The compound, which we call MFN103 or FFN103 depending on its use, has a reported log *D* of −1.98 and a pK_a of 5.95.

Ab initio Hartree-Fock calculations were performed as an initial proof of concept to predict the chemical shifts of the 5-F nucleus for the protonated (−130 ppm) and deprotonated (−126 ppm) states of the nearby 6-OH. A change in chemical shift of +4 ppm was predicted, using a gas-phase calculation and a limited 6-31 G** basis set. Additionally, BL3YP density functional theory calculations with the same basis set predicted a change in chemical shift of +14 ppm.

MFN 103 is a Functional False Neurotransmitter. To determine whether MFN103 fulfilled criterion #1 and if it is a substrate for DAT and/or VMAT2, we first tested its uptake in human embryonic kidney (HEK293) cells that express either DAT or both VMAT2 and DAT.[33] We observed a cell-filled staining pattern in the cells expressing only DAT and a more punctate staining pattern for the cells expressing both VMAT2 and DAT (Figure 2A). It is likely that VMAT2 is expressed on multiple membranes but is only functional on the membranes of acidic compartments, consistent with the punctate pattern.

We then tested MFN103 in an acute mouse brain slice using two-photon microscopy in the lateral dorsal striatum, a region of the brain innervated by dopaminergic axons projecting from the substantia nigra pars compacta. A mouse line that expresses green fluorescent protein driven by the TH promoter was used to determine the degree of colocalization of MFN103 to dopamine axons.[34] As shown in Figure 2B, MFN103 staining was mostly punctate with some visible strands that represent axons, a pattern identical to previously reported FFNs.[23,35,36] This pattern of label very closely overlapped: based on Costes' automatic threshold of three slice images from two different mice, there is a 0.37 ± 0.05 Pearson coefficient (compared to $r = 0.0 \pm 0$ for a randomized control, $p < 0.01$) between the MFN and TH-GFP signals, with 87.1 ± 0.4% of the blue MFN signal overlapping with the green GFP signal (M2).

Finally, striatal slices from wild-type mice were labeled with MFN103 following preincubation with nomifensine or reserpine (Figure 2C), competitive inhibitors of DAT and VMAT2, respectively. The punctate signal was decreased in

https://doi.org/10.1021/acschemneuro.1c00580
ACS Chem. Neurosci. 2021, 12, 4546−4553

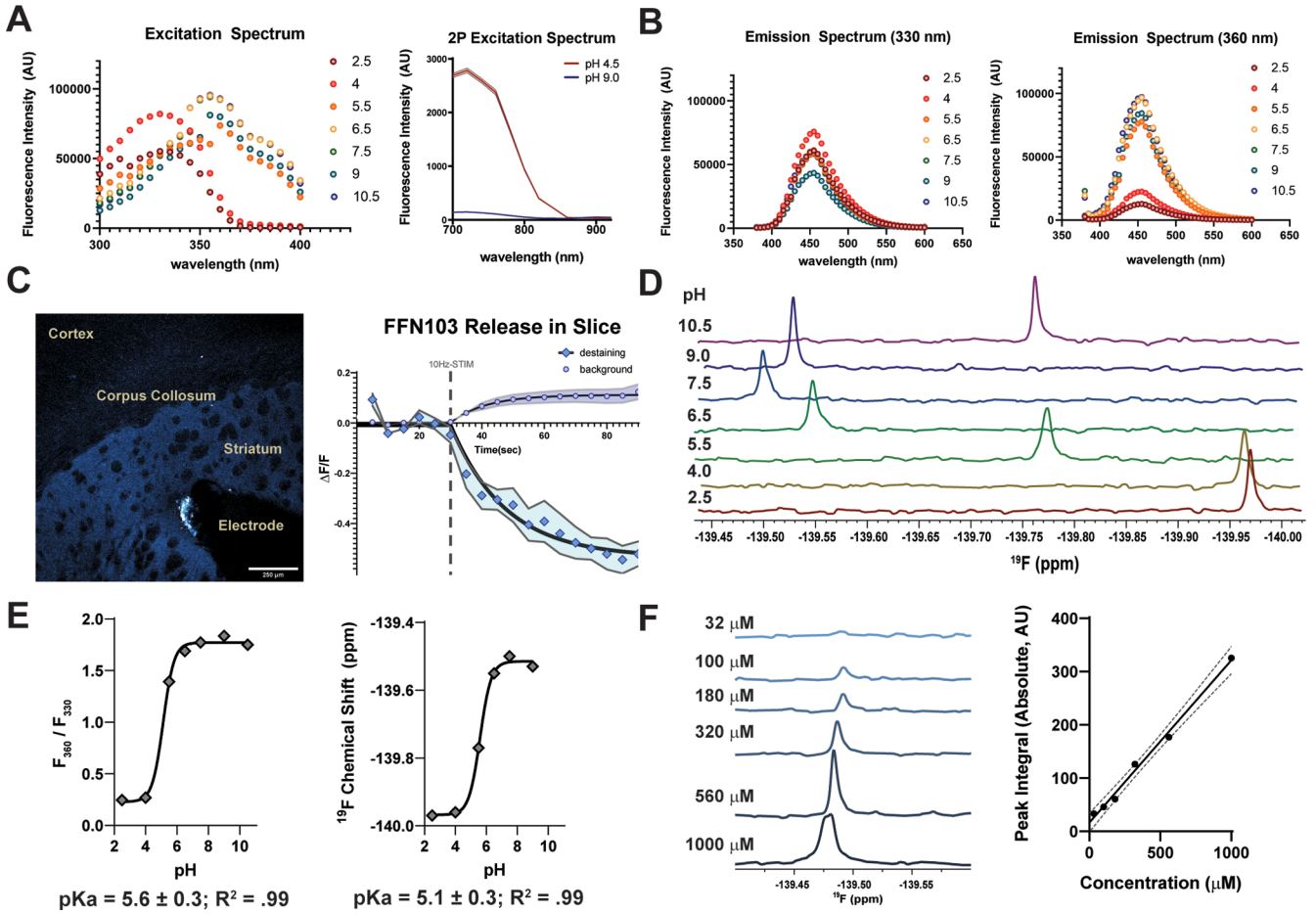

Figure 3. MFN103 is pH-sensitive. (A) Excitation spectrum collected on a fluorimeter (left) and 2P microscope (right) with emission set to 450 and (B) emission spectra with excitation set to 330 nm (left) and 360 nm (right) over a range of pH; (C) 2P image of the acute WT mouse striatum showing dopaminergic axon staining by MFN103 (left) and graph of fluorescence intensity over time before and during a 10 Hz stimulation train of both destaining puncta (diamonds) and background (circles); (D) 19F NMR spectra of MFN103 over a range of pH; (E) plot of the F360/F330 ratio (left) and chemical shifts (right) against pH; the data were fit to a sigmoidal curve and the calculated pK_a is shown below; and (F) 19F NMR spectra of MFN103 over a range of concentrations (left); the absolute integral of each peak was plotted against concentration to determine the detection limit.

the presence of inhibitors—29 ± 5 puncta and 19 ± 5 puncta for nomifensine and reserpine, respectively, compared to 410 ± 80 puncta per field of view. The signal intensity was only significantly lower in the nomifensine-treated slices and not in the reserpine-treated mice, consistent with accumulation into the axons by plasma membrane transport and accumulation into puncta by synaptic vesicle transport. Together, these data indicate that uptake into axons is indeed DAT- and VMAT2-dependent. We conclude from the HEK cell and striatal axon results data that MFN103 robustly satisfies the first criterion.

MFN103 is pH-Sensitive with a pK_a near 6. To analyze the second criterion that MFN103 is pH-sensitive with a pK in between the pH of a synaptic vesicle and the cytosolic space, excitation and emission spectra were acquired in PBS solutions of varying pH. As shown in Figure 3A, an excitation peak at 360 nm is dominant at basic-to-neutral pH. This peak decreases with pH as a peak at 330 nm builds in. Plotting the ratio of fluorescence intensity of these excitation wavelengths—F_{360}/F_{330}—against pH yields a sigmoidal curve that indicates a pK_a of 5.6 ± 0.3. Emission spectra, where the excitation wavelength is fixed to either 360 nm or 330 nm and the emission wavelength is swept, show a single peak at 455 nm regardless of excitation; there is a strong relationship between pH and fluorescent intensity, with neutral and basic pH demonstrating a nearly eightfold increase in fluorescence at neutral-basic pH (Figure 3B).

To further test MFN103's pH sensitivity, the probe was loaded into the acute mouse striatal slice as abovementioned to observe MFN release by multiphoton imaging. Release was induced by electrical stimulation with a concentric bipolar electrode placed within the tissue. A time series of 2.5 μm z-stack images were collected, first over a 30 s baseline period, before a 60 s train of 200 μA pulses was delivered at 10 Hz. The images were analyzed, with puncta sorted into "destaining" and "non-destaining" categories and analyzed for fluorescence intensity over time along with the background fluorescence intensity: we have previously demonstrated the presence of presynaptically silent axonal varicosities with synaptic vesicles in dopamine neuronal cultures, in the acute slices, and *in vivo* (see Methods).[23,36] As expected, the increase in fluorescence intensity observed at neutral pH for MFN103 resulted in an increase in background (nonpunctate) fluorescence upon stimulation, while the puncta themselves decreased in intensity following an exponential decay, as previously demonstrated with FFN102 and FFN270. The destaining puncta showed an exponential decay beginning at

https://doi.org/10.1021/acschemneuro.1c00580
ACS Chem. Neurosci. 2021, 12, 4546−4553

30 s that plateaued at a 52 ± 9% decrease in $\Delta F/F$. The non-destaining puncta showed no change in fluorescence, indicating a lack of signal bleaching under these conditions, while the overall signal increases in intensity by 11 ± 2% $\Delta F/F$ following stimulation, consistent with the class of flashing FFNs. Together with the fluorimeter data, these results demonstrate a functional pH dependence, satisfying the second criterion.

MFN103's pH Sensitivity Translates to 19F-MR. While we demonstrated that MFN103 is pH-sensitive, the experiments mentioned above do not test whether the fluorine handle vicinal to the hydroxy group experiences a change in chemical shift with changes in pH. Solutions of 500 μM MFN103 were made in Locke's buffer in a range of pH and spiked with D_2O and the 19F NMR reference sodium trifluoroacetate, which has a chemical shift of −76.55 ppm. Trifluoroacetate, which has a pK_a of 0.23, was used as a reference because it remains deprotonated at every pH tested.[37] These solutions were then scanned on a 500 MHz NMR spectrometer using a proton-decoupled 19F pulse sequence. Plotting chemical shift against pH reveals that the signal moves from −139.50 ppm at 9.0 and 7.5 pH to −139.69 at 4.0 and 2.5 pH, forming a sigmoidal curve analogous to the fluorimeter experiments. Interestingly, at pH 10.5, we see a chemical shift closer to that of pH 5 than the more basic solutions. This is likely due to deprotonation of the ethylamine group at high pH. Indeed, the comparable-in-structure phenethylamine has a pK_a of 9.73, and the deprotonated structure of MFN103 could be electronically different enough to cause this change in chemical shift.[38] We note that a pH of 10.5 is biologically irrelevant to the dopaminergic system and was not included when fitting a sigmoidal function to the plot, which yielded a pK_a of MFN103 of 5.1 ± 0.3, in agreement with the F360/F330 fit. This fulfills criteria number 3, as the 19F handle experiences a 0.5 ppm change in chemical shift when pH moves from physiological pH 7.5 to the synaptic pH of 4.5.

MFN103 Does Not Produce a Detectable MR Signal in Tissue. While the MFN signal can be detected in solution, we have not been able to record a signal to date in living cells using NMR, including in PC-12 cells, a cell line derived from a rat adrenal gland tumor often used to model catecholamine uptake as they express the peripheral secretory vesicle monoamine transporter VMAT1 and contain large dense core chromaffin secretory granules that are analogous to synaptic vesicles.[39,40] We also tested but were not able to record an MFN signal in DAT-transfected PC-12 cells, DAT- and/or VMAT2-expressing HEK cells, homogenized brain slices, or isolated synaptosomes. Our failure to measure an MFN signal in living cells can be due to at least two factors.

First, there may be insufficient NMR signal to observe in a 500 μL sample. While this could be in principle addressed using very long scan times (the largest number of scans attempted was 1024), this is stressful for experiments in cells in a standard NMR device. To determine the minimum concentration observable by NMR, using the same media and the same conditions as the in-cell experiments, we made solutions of MFN ranging from 32 to 1000 μM. Estimating the following—that there are 3×10^4 dopamine molecules per synaptic vesicle,[41] 80 vesicles per synapse,[42] 1×10^5 synapses per axon,[43] 2×10^5 dopaminergic axons in the striatum,[44] and a striatal volume of 25 μL[45]—we calculated a striatal dopamine concentration of 3 mM. Assuming a 10% replacement of dopamine with MFN (based on previous experiments),[23] we arrived at a final predicted concentration of 300 μM MFN in a mouse striatum. This concentration is well within the linear range observed and reported in Figure 3F; however, it is important to note that this is a conservative estimate, and a recent report by Peterson *et al.* suggested concentrations between 10 and 50 mM might be required for *in vivo* MRS detection.[46] The authors of that paper suggest that incorporating a paramagnetic metal into the design of the probe could increase the sensitivity as well as the magnitude of the pH-dependent change in chemical shift, which should be evaluated in future efforts.

Second, the vesicles in which MFN and dopamine accumulate could be very densely packed, which would preclude molecules from the ability to freely tumble as required for the generation of a free induction decay. To test this hypothesis, PC-12 cells were loaded, washed, resuspended, and sonicated in the presence of 0.1% Triton before scanning. Adding a detergent should degrade any membranes, thereby releasing the contents of any vesicles and allowing them to freely tumble in solution; however, even with this step, no signal was resolved, suggesting that the low concentration of the probe *in vivo* may be the dominant limiting factor.

CONCLUSIONS

As MR technology advances, with stronger magnets, better probes, and more advanced computing on the horizon, an MFN approach would be promising, as it could provide a rapid and noninvasive means to measure changes in monoamine neurotransmission, which would provide improved diagnosis, therapy, and understanding of normal function, with wide applicability to diseases including pheochromocytomas, Parkinson's and Huntington's diseases, schizophrenia, and affective disorders.

MFN103 is the first small molecule shown to fit the three criteria that would provide a functional magnetic resonance dopamine sensor: it is a VMAT2 and DAT substrate, is pH-sensitive with a pK_a ∼6, and has a fluorine handle with a chemical shift that moves 0.5 ppm from pH 4.5 to pH 7. It is limited in functionality, however, by the low sensitivity of 19F-MRS compared to fluorescence or PET, by the small concentrations in tissue, and by the single-fluorine design of the molecule. While imaging in larger organs in living animals—for example, the brain or adrenal glands—may provide a sufficient signal, this will require significant development, including toxicity studies and specialized MRS approaches, and may benefit from compounds with an increased signal.

We conclude that pH-sensitive FFNs can be modified into MFNs, although their successful measure in cells by resonance imaging requires further optimization. Future development might include the synthesis of FN structures with CF_3 moieties, which would in theory triple the signal, while more efficient substrates for VMAT2 might also increase the number of detectable nuclei in the sample.

METHODS

Calculations. 19F NMR chemical shift predictions were made using Spartan '14 (Wavefunction, Inc), molecules were constructed with the 6-OH group of MFN103 either protonated or deprotonated, and then, a ground-state calculation was made using Hartree-Fock or B3LYP density functional theory, each using a 6-31G** basis set, with

https://doi.org/10.1021/acschemneuro.1c00580
ACS Chem. Neurosci. 2021, 12, 4546−4553

NMR prediction enabled. The $\Delta\delta$ reported is the predicted ppm of the protonated species subtracted from the deprotonated species.

Two-Photon Imaging. HEK293T cells were cultured according to standard protocols, with complete medium consisting of Dulbecco's modified eagle medium supplemented with 10% fetal bovine serum, 1× glutamax, and 1× anti-biotic-antimycotic (Gibco | Thermofisher, Waltham, MA), and kept at 37 °C and 5% CO_2 in an incubator. WT cells were purchased from ATCC (Manassas, VA), and hDAT and hVMAT2-hDAT cells were a generous gift from Gary Miller's lab. Cells were split into 30 mm culture-treated dishes and grown to ∼80% confluency. On the day of imaging, media was replaced by 1 mL of fresh media and incubated for at least 1 h. Another 1 mL of complete media, containing 20−40 μM FN, was added to the dish (final conc: 10−20 μM) and incubated for 30 min. The media was aspirated and replaced with imaging media made with Fluorobrite DMEM (Gibco), which lacks phenol red, and incubated for 15−30 min to wash out nonspecific labeling. The imaging media was replaced once more before imaging.

Acute brain slices were prepared essentially as described in Lieberman *et al.*[47] Briefly, mice underwent cervical dislocation and the brain was removed and placed in ice-cold high sucrose cutting solution (in mM): 10 NaCl, 2.5 KCl, 25 $NaHCO_3$, 0.5 $CaCl_2$, 7 $MgCl_2$, 1.25 NaH_2PO_4, 180 sucrose, and 10 glucose bubbled with 95% O_2/5% CO_2 to pH 7.4. Brains were mounted on a VT1200 vibratome (Leica Biosystems), and coronal sections (250 μm) containing the striatum were collected. Slices were moved to holding jars containing ACSF (in mM): 125 NaCl, 2.5 KCl, 25 $NaHCO_3$, 2 $CaCl_2$, 1 $MgCl_2$, 1.25 NaH_2PO_4, and 10 glucose bubbled with 95% O_2/5% CO_2 at 34 °C for 30 min and then to room temperature for the duration of experiments. To label with FFNs, slices were moved to a beaker containing 5 mL of 10 μM FFN103 for 30 min, followed by a 15−30 min wash in ACSF before imaging.

All images were acquired on a Prairie Ultima microscope system (Middleton, WI) using PrairieView 4.5 software. Acute brain slices were transferred into a chamber and perfused with oxygenated ACSF at room temperature; HEK cells were imaged in their respective dishes. Samples were excited with a Coherent Chameleon Ultra two-photon laser (Santa Clara, CA) at 760 nm for FFNs or 920 nm for GFP, and images were simultaneously collected through two photomultiplier tube channels with corresponding 460 ± 25 and 525 ± 25 nm emission windows. The objective used was a 60 × 0.9 NA or 10 × 0.3 NA water immersion lens, and images were 1024 × 1024 pixels in size. For stimulation experiments, a 256 × 256 px ROI was used and 2.5 μm/0.5 μm z-stacks were collected every 5 s.

All data were analyzed in ImageJ (NIH, FIJI build). The JACOP plugin was used for co-localization calculations,[48] and puncta were selected using the Multiple Thresholds Parameters v3.5 macro.[49] For stimulation experiments, images were registered using Correct 3D drift plugin and flattened using Z-project, average intensity. Puncta from the first time point were identified, and an inverse selection was made to identify and measure the fluorescence intensity of the background at each time point. Subtract background processing was applied at 10 px rolling ball, and then, the mean intensity for each punctum was measured at each time point. $\Delta F/F$ was calculated by averaging the first six time points and normalizing each point to that average. Each punctum time course was then fit for a delayed exponential decay function. Puncta were sorted into three categories: destaining puncta had an exponential decay fit with $R^2 > 0.6$, an X0 parameter between 25 and 30 s, and an asymptote <−0.2 $\Delta F/F$; non-destaining puncta had a mean $\Delta F/F$ within ±5% over the course of the stimulation; other signals were considered drifting, anomalous, or nonpunctate and were not included in analysis.

Fluorescence and NMR Spectroscopy. Fluorescence intensity measurements were made on a SpectraMax M3 plate reader (Molecular Devices, San Jose, CA) on black opaque 96-well plates or in quartz cuvettes. NMR experiments were performed on a 500 MHz AV-III scanner (Bruker, Billerica, MA). For the fluorimeter, samples were made in Locke's buffer (in mM): 154 NaCl, 5.6 KCl, 3.6 $NaHCO_3$, 2.3 $CaCl_2$, 5 HEPES acid, 5.6 glucose, pH = 7.4. For NMR, a 1.1× solution of Locke's was made and then diluted to 1× with 10% D_2O and supplemented with 500 μM NaF_3COO. NMR data were analyzed using MestReNova 14.2. The trifluoroacetate peak was set to −76.

For in-cell NMR experiments, nonadherent PC-12 cells (ATCC, Manassas, VA) were cultured in RPMI (ATCC) supplemented with 10% horse serum and 5% FBS (Gibco). Two days before an experiment, cells were split into T75 flasks at 1 million cells in 15 mL. Forty-eight hours later, cells were incubated with MFN103 or DMSO as a negative control for 1 h at 37 °C in 5% CO_2 and then spun down and resuspended them in Locke's buffer both to remove nonspecific labeling and to transfer them to a media compatible with fluorescence or NMR experiments. Both conditions were verified on a fluorimeter by comparing their fluorescence intensity at 330 nm and 360 nm, with the MFN-treated cells having a significantly higher fluorescence intensity at both wavelengths than the DMSO-treated cells. To analyze the cells by NMR, Locke's buffer was prepared with 10% D_2O and 500 μM sodium trifluoroacetate to serve as a reference. The cells were resuspended into 500 μL and then transferred to an NMR tube and scanned. No signal was observed between −139 and −140 ppm.

Data Analysis and Statistics. All data were organized in Microsoft Excel and analyzed in Graphpad Prism. All error bars/bands represent standard error of the mean (SEM). Errors reported for fits (such as pK_a) are reported as 95% confidence intervals.

AUTHOR INFORMATION

Corresponding Authors

Dalibor Sames − *Department of Chemistry, Columbia University, New York, New York 10027, United States;* orcid.org/0000-0001-6911-2260; Email: ds584@columbia.edu

David Sulzer − *Department of Psychiatry, Columbia University, Division of Molecular Therapeutics, New York State Psychiatric Institute, New York, New York 10032, United States; Departments of Neurology and Pharmacology, Columbia University, New York, New York 10032, United States;* orcid.org/0000-0001-7632-0439; Email: ds43@cumc.columbia.edu

Authors

Michael R. Post − *Department of Psychiatry, Columbia University, Division of Molecular Therapeutics, New York State Psychiatric Institute, New York, New York 10032, United States*

Wei-Li Lee − *Department of Chemistry, Columbia University, New York, New York 10027, United States*

Jia Guo − *Department of Psychiatry, Columbia University, Division of Molecular Therapeutics, New York State Psychiatric Institute, New York, New York 10032, United States*

Complete contact information is available at: https://pubs.acs.org/10.1021/acschemneuro.1c00580

Author Contributions

M.R.P. and D.Sulzer designed research; M.R.P. and W.-L.L. performed research; J.G. contributed to, advised, and supported unpublished *in vivo* MRS studies; D.Sames and D.Sulzer advised, supported, and guided research; and M.R.P. analyzed data and wrote the paper.

Notes

The authors declare no competing financial interest.

ACKNOWLEDGMENTS

We would like to thank Art Palmer and Larry Kegeles, for their advice, time, and contributions to in-cell magnetic resonance experiments and Gary Miller for his counsel and VMAT/DAT

cell lines. Funding for this work was provided by the NIH (D.Sames &D.Sulzer: R01MH108186; D.Sulzer: DA007418; M.R.P.: T32MH20004, K99MH122659) and the JPB foundation (D.Sulzer: 1210).

REFERENCES

(1) Hodge, G. K.; Butcher, L. L. Pars Compacta of the Substantia Nigra Modulates Motor Activity but Is Not Involved Importantly in Regulating Food and Water Intake. *N. Schmied. Arch. Pharmacol.* **1980**, *313*, 51−67.
(2) Morales, M.; Margolis, E. B. Ventral Tegmental Area: Cellular Heterogeneity, Connectivity and Behaviour. *Nat. Rev. Neurosci.* **2017**, *18*, 73−85.
(3) Bohnen, N. I.; Albin, R. L. The Cholinergic System and Parkinson Disease. *Behav. Brain Res.* **2011**, *221*, 564−573.
(4) Howes, O. D.; Murray, R. M. Schizophrenia: An Integrated Sociodevelopmental-Cognitive Model. *The Lancet* **2014**, *383*, 1677−1687.
(5) Abi-Dargham, A.; Horga, G. The Search for Imaging Biomarkers in Psychiatric Disorders. *Nat. Med.* **2016**, *22*, 1248−1255.
(6) Edwards, R. H. The Neurotransmitter Cycle and Quantal Size. *Neuron* **2007**, *55*, 835−858.
(7) Guillot, T. S.; Miller, G. W. Protective Actions of the Vesicular Monoamine Transporter 2 (VMAT2) in Monoaminergic Neurons. *Mol. Neurobiol.* **2009**, *39*, 149−170.
(8) Knoth, J.; Zallakian, M.; Njus, D. Stoichiometry of Hydrogen Ion-Linked Dopamine Transport in Chromaffin Granule Ghosts. *Biochemistry* **1981**, *20*, 6625−6629.
(9) Lohr, K. M.; Bernstein, A. I.; Stout, K. A.; Dunn, A. R.; Lazo, C. R.; Alter, S. P.; Wang, M.; Li, Y.; Fan, X.; Hess, E. J.; Yi, H.; Vecchio, L. M.; Goldstein, D. S.; Guillot, T. S.; Salahpour, A.; Miller, G. W. Increased Vesicular Monoamine Transporter Enhances Dopamine Release and Opposes Parkinson Disease-Related Neurodegeneration in Vivo. *Proc. Natl. Acad. Sci.* **2014**, *111*, 9977−9982.
(10) Hersch, S. M.; Yi, H.; Heilman, C. J.; Edwards, R. H.; Levey, A. I. Subcellular Localization and Molecular Topology of the Dopamine Transporter in the Striatum and Substantia Nigra. *J. Comp. Neurol.* **1997**, *388*, 2112−2274.
(11) Sulzer, D.; Cragg, S. J.; Rice, M. E. Striatal Dopamine Neurotransmission: Regulation of Release and Uptake. *Basal Ganglia* **2016**, *6*, 123−148.
(12) Berke, J. D. What Does Dopamine Mean? *Nat. Neurosci.* **2018**, *21*, 787−793.
(13) Post, M. R.; Sulzer, D. The Chemical Tools for Imaging Dopamine Release. *Cell Chem. Biol.* **2021**, *28*, 748−764.
(14) Kanthan, M.; Cumming, P.; Hooker, J. M.; Vasdev, N. Classics in Neuroimaging: Imaging the Dopaminergic Pathway with PET. *ACS Chem. Neurosci.* **2017**, *8*, 1817−1819.
(15) Labouesse, M. A.; Cola, R. B.; Patriarchi, T. GPCR-Based Dopamine Sensors-A Detailed Guide to Inform Sensor Choice for In Vivo Imaging. *Int. J. Mol. Sci.* **2020**, *21*, 8048.
(16) Lee, T.; Cai, L. X.; Lelyveld, V. S.; Hai, A.; Jasanoff, A. Molecular-Level Functional Magnetic Resonance Imaging of Dopaminergic Signaling. *Science* **2014**, *344*, 533−535.
(17) Patriarchi, T.; Cho, J. R.; Merten, K.; Howe, M. W.; Marley, A.; Xiong, W.-H.; Folk, R. W.; Broussard, G. J.; Liang, R.; Jang, M. J.; Zhong, H.; Dombeck, D.; von Zastrow, M.; Nimmerjahn, A.; Gradinaru, V.; Williams, J. T.; Tian, L. Ultrafast Neuronal Imaging of Dopamine Dynamics with Designed Genetically Encoded Sensors. *Science* **2018**, *360*, No. eaat4422.
(18) Sun, F.; Zeng, J.; Jing, M.; Zhou, J.; Feng, J.; Owen, S. F.; Luo, Y.; Li, F.; Wang, H.; Yamaguchi, T.; Yong, Z.; Gao, Y.; Peng, W.; Wang, L.; Zhang, S.; Du, J.; Lin, D.; Xu, M.; Kreitzer, A. C.; Cui, G.; Li, Y. A Genetically Encoded Fluorescent Sensor Enables Rapid and Specific Detection of Dopamine in Flies, Fish, and Mice. *Cell* **2018**, *174*, 481−496.e19.
(19) Kruss, S.; Landry, M. P.; Vander Ende, E.; Lima, B. M. A.; Reuel, N. F.; Zhang, J.; Nelson, J.; Mu, B.; Hilmer, A.; Strano, M. Neurotransmitter Detection Using Corona Phase Molecular Recognition on Fluorescent Single-Walled Carbon Nanotube Sensors. *J. Am. Chem. Soc.* **2014**, *136*, 713−724.
(20) Shapiro, M. G.; Westmeyer, G. G.; Romero, P. A.; Szablowski, J. O.; Küster, B.; Shah, A.; Otey, C. R.; Langer, R.; Arnold, F. H.; Jasanoff, A. Directed Evolution of a Magnetic Resonance Imaging Contrast Agent for Noninvasive Imaging of Dopamine. *Nat. Biotechnol.* **2010**, *28*, 264−270.
(21) Li, N.; Jasanoff, A. Local and Global Consequences of Reward-Evoked Striatal Dopamine Release. *Nature* **2020**, *580*, 239−244.
(22) Sames, D.; Dunn, M.; Karpowicz, R. J.; Sulzer, D. Visualizing Neurotransmitter Secretion at Individual Synapses. *ACS Chem. Neurosci.* **2013**, *4*, 648−651.
(23) Lee, M.; Gubernator, N. G.; Sulzer, D.; Sames, D. Development of PH-Responsive Fluorescent False Neurotransmitters. *J. Am. Chem. Soc.* **2010**, *132*, 8828−8830.
(24) Dunn, M.; Henke, A.; Clark, S.; Kovalyova, Y.; Kempadoo, K. A.; Karpowicz, R. J.; Kandel, E. R.; Sulzer, D.; Sames, D. Designing a Norepinephrine Optical Tracer for Imaging Individual Noradrenergic Synapses and Their Activity in Vivo. *Nat. Commun.* **2018**, *9*, 2838.
(25) Sulzer, D.; Sonders, M. S.; Poulsen, N. W.; Galli, A. Mechanisms of Neurotransmitter Release by Amphetamines: A Review. *Prog. Neurobiol.* **2005**, *75*, 406−433.
(26) Prost, R. W. Magnetic resonance spectroscopy. *Med. Phys.* **2008**, *35*, 4530−4544.
(27) Öngür, D. Making Progress With Magnetic Resonance Spectroscopy. *JAMA Psychiatry* **2013**, *70*, 1265.
(28) Rothman, D. L.; Petroff, O. A.; Behar, K. L.; Mattson, R. H. Localized 1H NMR Measurements of Gamma-Aminobutyric Acid in Human Brain in Vivo. *Proc. Natl. Acad. Sci.* **1993**, *90*, 5662−5666.
(29) Guo, J.; Gang, Z.; Sun, Y.; Laine, A.; Small, S. A.; Rothman, D. L. In Vivo Detection and Automatic Analysis of GABA in the Mouse Brain with MEGA-PRESS at 9.4 T. *NMR Biomed* **2018**, *31*, No. e3837.
(30) Diffley, D. M.; Costa, J. L.; Sokoloski, E. A.; Chiueh, C. C.; Kirk, K. L.; Creveling, C. R. Direct Observation of 6-Fluorodopamine in Guinea Pig Nerve Microsacs by 19F NMR. *Biochem. Biophys. Res. Commun.* **1983**, *110*, 740−745.
(31) Yamaguchi, K.; Ueki, R.; Nonaka, H.; Sugihara, F.; Matsuda, T.; Sando, S. Design of Chemical Shift-Switching 19F Magnetic Resonance Imaging Probe for Specific Detection of Human Monoamine Oxidase A. *J. Am. Chem. Soc.* **2011**, *133*, 14208−14211.
(32) Wolf, W.; Albright, M. J.; Silver, M. S.; Weber, H.; Reichardt, U.; Sauer, R. Fluorine-19 NMR Spectroscopic Studies of the Metabolism of 5-Fluorouracil in the Liver of Patients Undergoing Chemotherapy. *Magn. Reson. Imaging* **1987**, *5*, 165−169.
(33) Bernstein, A. I.; Stout, K. A.; Miller, G. W. A Fluorescent-Based Assay for Live Cell, Spatially Resolved Assessment of Vesicular Monoamine Transporter 2-Mediated Neurotransmitter Transport. *J. Neurosci. Methods* **2012**, *209*, 357−366.
(34) Gong, S.; Zheng, C.; Doughty, M. L.; Losos, K.; Didkovsky, N.; Schambra, U. B.; Nowak, N. J.; Joyner, A.; Leblanc, G.; Hatten, M. E.; Heintz, N. A Gene Expression Atlas of the Central Nervous System Based on Bacterial Artificial Chromosomes. *Nature* **2003**, *425*, 917−925.
(35) Gubernator, N. G.; Zhang, H.; Staal, R. G. W.; Mosharov, E. V.; Pereira, D. B.; Yue, M.; Balsanek, V.; Vadola, P. A.; Mukherjee, B.; Edwards, R. H.; Sulzer, D.; Sames, D. Fluorescent False Neurotransmitters Visualize Dopamine Release from Individual Presynaptic Terminals. *Science* **2009**, *324*, 1441−1444.
(36) Pereira, D. B.; Schmitz, Y.; Mészáros, J.; Merchant, P.; Hu, G.; Li, S.; Henke, A.; Lizardi-Ortiz, J. E.; Karpowicz, R. J.; Morgenstern, T. J.; Sonders, M. S.; Kanter, E.; Rodriguez, P. C.; Mosharov, E. V.; Sames, D.; Sulzer, D. Fluorescent False Neurotransmitter Reveals Functionally Silent Dopamine Vesicle Clusters in the Striatum. *Nat. Neurosci.* **2016**, *19*, 578−586.
(37) Okaru, A. O.; Brunner, T. S.; Ackermann, S. M.; Kuballa, T.; Walch, S. G.; Kohl-Himmelseher, M.; Lachenmeier, D. W. Application of 19F NMR Spectroscopy for Content Determination

https://doi.org/10.1021/acschemneuro.1c00580
ACS Chem. Neurosci. 2021, 12, 4546−4553

of Fluorinated Pharmaceuticals. *J. Anal. Methods Chem.* **2017**, *2017*, 9206297.
(38) *CRC Handbook of Chemistry and Physics: A Ready-Reference Book of Chemical and Physical Data, 63*; Weast, R. C., Ed.; CRC Press: Boca Raton, Fla, 1983.
(39) Greene, L. A.; Tischler, A. S. Establishment of a Noradrenergic Clonal Line of Rat Adrenal Pheochromocytoma Cells Which Respond to Nerve Growth Factor. *Proc. Natl. Acad. Sci.* **1976**, *73*, 2424−2428.
(40) Westerink, R. H. S.; Ewing, A. G. The PC12 cell as model for neurosecretion. *Acta Physiol.* **2007**, *192*, 273−285.
(41) Pothos, E. N.; Davila, V.; Sulzer, D. Presynaptic Recording of Quanta from Midbrain Dopamine Neurons and Modulation of the Quantal Size. *J. Neurosci.* **1998**, *18*, 4106−4118.
(42) Ikeda, K.; Bekkers, J. M. Counting the Number of Releasable Synaptic Vesicles in a Presynaptic Terminal. *Proc. Natl. Acad. Sci.* **2009**, *106*, 2945−2950.
(43) Matsuda, W.; Furuta, T.; Nakamura, K. C.; Hioki, H.; Fujiyama, F.; Arai, R.; Kaneko, T. Single Nigrostriatal Dopaminergic Neurons Form Widely Spread and Highly Dense Axonal Arborizations in the Neostriatum. *J. Neurosci.* **2009**, *29*, 444−453.
(44) Nair-Roberts, R. G.; Chatelain-Badie, S. D.; Benson, E.; White-Cooper, H.; Bolam, J. P.; Ungless, M. A. Stereological Estimates of Dopaminergic, GABAergic and Glutamatergic Neurons in the Ventral Tegmental Area, Substantia Nigra and Retrorubral Field in the Rat. *Neuroscience* **2008**, *152*, 1024−1031.
(45) Badea, A.; Ali-Sharief, A. A.; Johnson, G. A. Morphometric Analysis of the C57BL/6J Mouse Brain. *NeuroImage* **2007**, *37*, 683−693.
(46) Peterson, K. L.; Srivastava, K.; Pierre, V. C. Fluorinated Paramagnetic Complexes: Sensitive and Responsive Probes for Magnetic Resonance Spectroscopy and Imaging. *Front. Chem.* **2018**, *6*, 160.
(47) Lieberman, O. J.; Cartocci, V.; Pigulevskiy, I.; Molinari, M.; Carbonell, J.; Broseta, M. B.; Post, M. R.; Sulzer, D.; Borgkvist, A.; Santini, E. MTOR Suppresses Macroautophagy During Striatal Postnatal Development and Is Hyperactive in Mouse Models of Autism Spectrum Disorders. *Front. Cell. Neurosci.* **2020**, *14*, 70.
(48) Bolte, S.; Cordelières, F. P. A Guided Tour into Subcellular Colocalization Analysis in Light Microscopy. *J. Microsc.* **2006**, *224*, 213−232.
(49) Mojard Kalkhoran, S.; Chow, S. H. J.; Walia, J. S.; Gershome, C.; Saraev, N.; Kim, B.; Poburko, D. VNUT and VMAT2 Segregate within Sympathetic Varicosities and Localize near Preferred Cav2 Isoforms in the Rat Tail Artery. *Am. J. Physiol.: Heart Circ. Physiol.* **2019**, *316*, H89−H105.

https://doi.org/10.1021/acschemneuro.1c00580
ACS Chem. Neurosci. 2021, 12, 4546−4553